A 9.4 GHZ INTRINSICALLY SWITCHABLE LAMB-WAVE RESONATOR USING ATOMIC-LAYER-DEPOSITED FERROELECTRIC HAFNIA-ZIRCONIA

Troy Tharpe and Roozbeh Tabrizian*
Department of Electrical and Computer Engineering, University of Florida, USA

ABSTRACT

This paper reports the first-ever demonstration of a 9.4 GHz Lamb-wave resonator with intrinsic switchability in atomic-layer-deposited (ALD) ferroelectric hafnia-zirconia ($Hf_{0.5}Zr_{0.5}O_2$) films. The resonator is comprised of a 50nm-thick laminated $Hf_{0.5}Zr_{0.5}O_2$ transducer, sandwiched between ~20nm-thick tungsten (W) electrodes. The high resonance frequency is achieved by exciting asymmetric shear-based Lamb-waves, using the rotated polar axis of $Hf_{0.5}Zr_{0.5}O_2$, and with a frequency defined primarily by the transducer thickness. Intrinsic switchability is achieved by nulling the instantaneous polarization of the $Hf_{0.5}Zr_{0.5}O_2$, thanks to the ferroelectric behavior of the film. The resonator prototype demonstrates a quality factor (Q) of 314 and an electromechanical coupling factor (k_t^2) of 0.31% and is intrinsically switched through application of a 10.5V DC. Relying on a standard-CMOS materials and process, along with the very high resonance frequency and the intrinsic switchability, $Hf_{0.5}Zr_{0.5}O_2$ Lamb-wave resonators highlight the promise for creation of CMOS-monolithic frequency references over cm- and mm-wave regimes.

KEYWORDS

Ferroelectric, hafnia-zirconia, Lamb-wave, resonator, intrinsic, switchability, super high frequency.

INTRODUCTION

Micro- and nano-acoustic resonators are vital for creation of chip-scale clocks, frequency references, and spectral processors in modern electronic systems. Q's that are multiple orders of magnitude higher than integrated passives make these resonators superior [1][2]. However, the non-monolithic integration, due to CMOS incompatible fabrication process, and the quality degradation of conventional (*e.g.*, sputtered) piezoelectric films upon miniaturization for frequency scaling, set major barriers for adoption of acoustic resonators in cm- and mm-wave frequency control systems. Further, the exponential increase in wireless traffic volume and corresponding increase in number of frequency bands expose a substantial footprint challenge for current non-monolithic integration approaches.

Despite these inherent drawbacks and challenges, the discovery of ferroelectricity in hafnia [3], along with the first demonstration of ferroelectric hafnia-zirconia as a nanoelectromechanical transducer [4][5][6], augur a promising solution for monolithic integration of high-Q nano-acoustic resonators in advanced semiconductor nodes. Benefiting from the inherent CMOS compatibility and outstanding thickness scalability to sub-5nm [7], ALD ferroelectric hafnia-zirconia films are poised to realize CMOS-monolithic super- and extremely-high frequency nano-acoustic resonators integrated in front- or back-end-of-line (FEOL / BEOL). Here, we demonstrate this potential by presenting the first super-high-frequency ALD hafnia-zirconia resonator, and further demonstrate the intrinsic switchability feature that is enabled by ferroelectricity.

HAFNIA-ZIRCONIA TRANSDUCER

Ferroelectricity, and therefore piezoelectricity within $Hf_{0.5}Zr_{0.5}O_2$ corresponds to the formation of the noncentrosymmetric, polar orthorhombic crystal phase (space group $Pca2_1$) [8][9], stabilized through application of biaxial stress

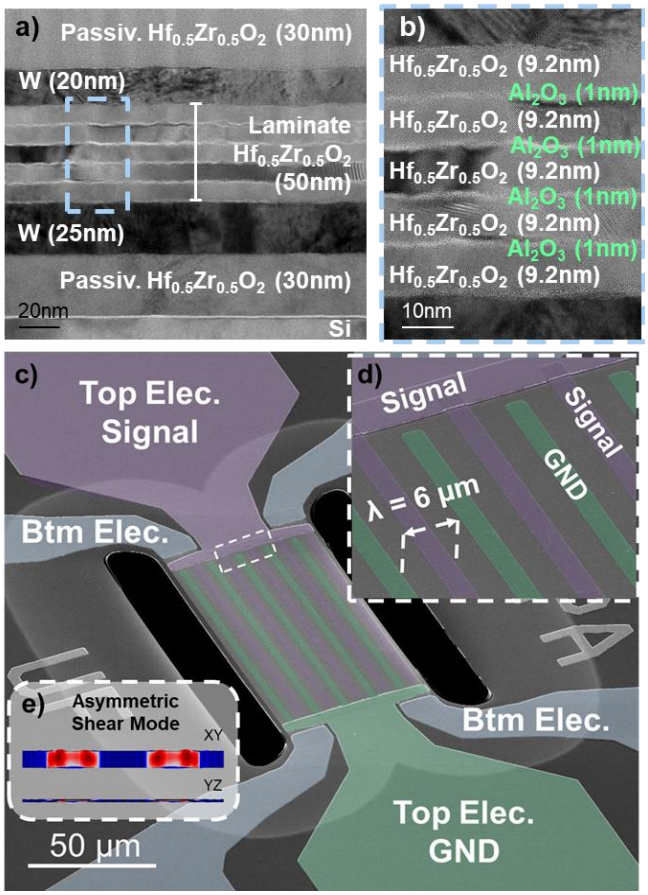

Figure 1. *a) TEM image of the resonant stack with constituent layer material and thickness annotated. b) Small scale TEM image highlighting individual layers of the 50nm, $Hf_{0.5}Zr_{0.5}O_2$ laminate transducer. c) SEM image of a 9.4 GHz intrinsically switchable, $Hf_{0.5}Zr_{0.5}O_2$ Lamb-mode resonator. d) Small-scale SEM highlighting electrode configuration and 6 µm IDT pitch. e) Asymmetric, shear BAW resonance mode.*

[10][11] and limitation of grain size [12]. To provide this environment for ferroelectricity, the 50nm $Hf_{0.5}Zr_{0.5}O_2$ transducer is formed via alternating ALD of 9.2nm $Hf_{0.5}Zr_{0.5}O_2$ and 1nm of Al_2O_3 to limit grain size during crystallization. Crystallization is achieved by rapid thermal anneal (RTA) for 20s in nitrogen ambient, with W electrodes serving as mechanical boundary. Figure 1 (a) depicts a transmission electron microscope (TEM) image of the resonator cross section, while Fig. 1 (b) shows a TEM image highlighting the 50nm, laminate $Hf_{0.5}Zr_{0.5}O_2$ transducer.

Thickness scaling of the $Hf_{0.5}Zr_{0.5}O_2$ transducer to 50nm and beyond is favorable for a larger measurable displacement upon application of electromagnetic field [13]. To verify ferroelectric behavior and electromechanical coupling (post RTA), polarization and displacement hysteresis loops for 20nm W/ 50nm $Hf_{0.5}Zr_{0.5}O_2$/ 25nm W capacitors are measured using a Radiant PiezoMEMS analyzer and NLV laser vibrometer. Figure 2 depicts polarization

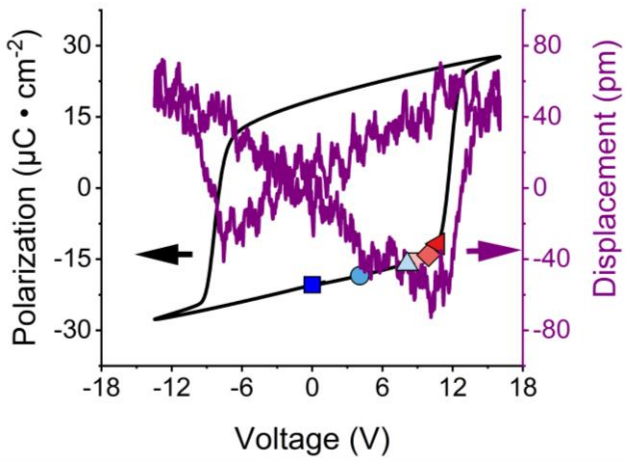

Figure 2. *Polarization and displacement hysteresis loops for a 0.0025 cm² W/ $Hf_{0.5}Zr_{0.5}O_2$/ W capacitor with thickness dimensions noted in Figure 1. d). Highlighted bias voltages correspond to measurement conditions in Figure 4.*

and displacement loops for an unreleased, 0.0025cm² capacitor with cross section identical to fabricated Lamb-wave prototypes, after application of 1,000 cycles of a 15V, 1kHz, square wakeup pulse. Highlighted voltages represent (from left to right) 0V, 4V, 8V, 8.6V, 9.4V, and 10.5V and relate to resonator admittance measurements taken at port 1 subject to corresponding bias.

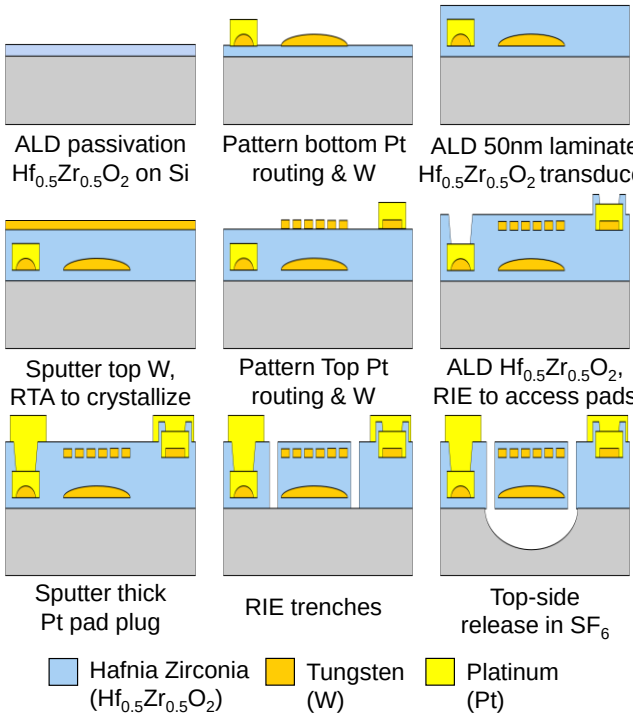

Figure 3. *CMOS-compatible fabrication process to realize $Hf_{0.5}Zr_{0.5}O_2$ Lamb-mode resonators.*

FABRICATION PROCESS

Figure 3 summarizes the nine-step, CMOS compatible fabrication process flow used to realize $Hf_{0.5}Zr_{0.5}O_2$ Lamb-mode resonator prototypes.

Starting with a high resistivity silicon (Si) wafer, 30nm of $Hf_{0.5}Zr_{0.5}O_2$ passivation layer is deposited via ALD using tetrakis(dimethylamido)hafnium(IV) (TDMAH) and tetrakis(dimethylamido)zirconium(IV) (TDMAZ) precursors with a cycle ratio of 1:1. Application of hydrogen and oxygen plasmas at 300W with each monolayer, oxidizes the layer and promotes the formation of orthorhombic phase during subsequent RTA [14][15]. This bottom passivation layer is so named as it protects bottom electrode layers during future release steps. Next 25nm of W is sputtered and patterned using a sulfur hexafluoride (SF_6) and argon reactive ion etch (RIE) recipe to form resonator bottom electrodes, while 150nm of platinum (Pt) is lifted off for bottom routing. Then, the nanolaminate transducer is formed via ALD of 5x 9.2 nm $Hf_{0.5}Zr_{0.5}O_2$ layers, intercalated with 4x 1nm thermal Al_2O_3, using trimethylaluminum (TMA) precursor. Top 20nm W is then sputtered and RTA performed. Subsequently, top device electrodes are pattered using RIE, and top 150nm Pt routing is again lifted off. A symmetric, top 30nm ALD $Hf_{0.5}Zr_{0.5}O_2$ passivation layer is then deposited to again protect the resonant body during release. Access to top and bottom Pt pads are etched using a chlorine (Cl_2), Ar gas chemistry in RIE and thick, 200nm Pt pad plugs are lifted off to form a low resistance resonator contact point. Finally, resonator trenches are defined using a Cl_2 / Ar RIE etch, and the device is released via topside etching of Si using SF_6.

RESONATOR OPERATION MODE

The presented $Hf_{0.5}Zr_{0.5}O_2$, resonators have been primarily designed for excitation of symmetric Lamb modes with predominantly extensional elastic fields. However, due to the unique texturing process of $Hf_{0.5}Zr_{0.5}O_2$ upon annealing and wake-up cycling [16][17], a non-normal (*i.e.*, rotated) polar- / c-axis is achieved that enables excitation of asymmetric modes upon application of electric field across the thickness. In particular, the rotated polar axis enables excitation of an asymmetric Lamb wave with predominant thickness-shear content at 9.4 GHz. Figure 1 (c) depicts a scanning electron microscope (SEM) image of the released resonator prototype. The one-port resonator is configured with one pair of interdigitated transducers (IDTs) connected to a drive signal (highlighted purple), with another IDT pair connected to ground (highlighted green). A floating device bottom electrode (highlighted blue) allows for application of uniform electric field across the thickness of $Hf_{0.5}Zr_{0.5}O_2$ transducer. Considering the rotated polar axis of the film, the vertical electric field enables excitation of both thickness-extensional and thickness-shear waves through the longitudinal piezoelectric coefficient (d_{33}). Figure 1 (d) depicts a small-scale SEM image of the realized Lamb-mode resonator's top electrode, denoting IDT configuration. Figure 1 (e) shows the COMSOL simulated, asymmetric shear mode of excitation, with a polar c-axis tilt of 34º, and frequency primarily defined by transducer thickness.

RESONATOR CHARACTERIZATION

Admittance ($|Y_{11}|$) responses of the presented $Hf_{0.5}Zr_{0.5}O_2$, Lamb-wave resonator are taken using a Keysight N522A vector network analyzer, with a variable DC bias applied to port 1 via bias-Tee network and benchtop DC source. Figure 4 (a) depicts measured $|Y_{11}|$ responses for the resonator presented in Figure 1 (c). Of note, is the coloring and symbology of applied bias voltage, which can be mapped to points denoted on the polarization hysteresis loop displayed in Fig. 2. In the On state (0V DC applied), a Q of 314 and a k_t^2 of 0.31% is measured for the mode at 9.4 GHz. While the Off state corresponds to the application of 10.5V DC, in which the

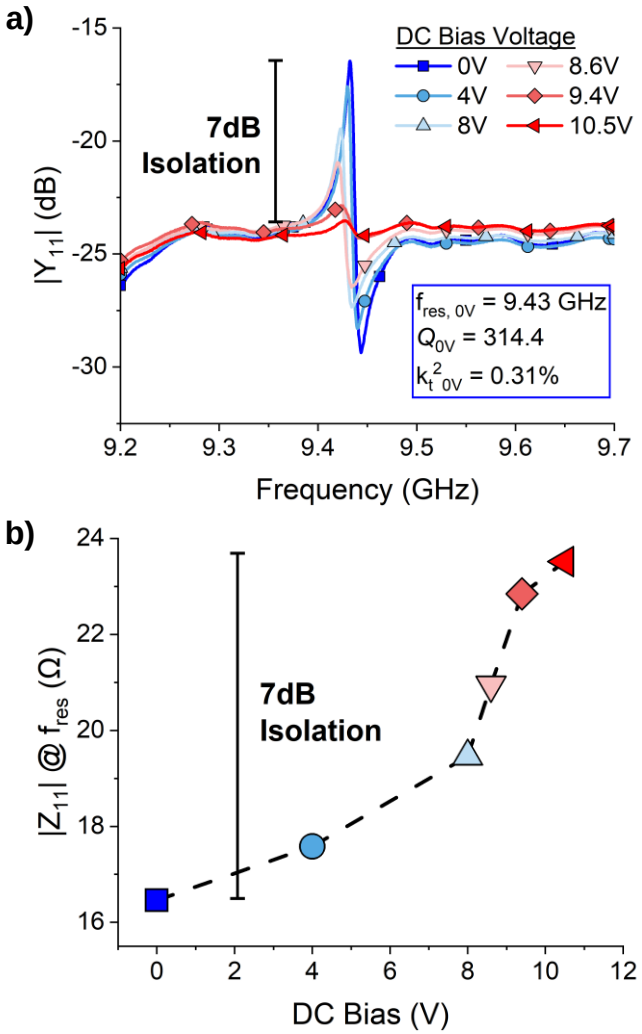

Figure 4. *a) Measured admittance of the device shown in Figure 1. c) taken at varied DC bias. As voltages near coercive and the $Hf_{0.5}Zr_{0.5}O_2$ film depolarizes, the asymmetric, shear, Lamb-mode switches off with 7dB of isolation. b) The magnitude of impedance ($|Z_{11}|$) at resonance for varied DC bias.*

transducer is nearly depolarized, nulling the electromechanical coupling and resulting in ~7dB of on/off isolation. Figure 4. (b) relates bias voltages to impedance values ($|Z_{11}|$).

ELECTROMECHANICAL COUPLING DISCUSSION

The extracted k_t^2 of 0.31% is appreciably smaller than expected for Lamb-mode resonators transduced by $Hf_{0.5}Zr_{0.5}O_2$, owing to $Hf_{0.5}Zr_{0.5}O_2$'s large reported d_{33} coefficient [13]. This lower-than-expected coupling is due to the reversion of polar orthorhombic phase to non-polar monoclinic phase upon resonator release, as first reported elsewhere [18]. With the polar orthorhombic phase of $Hf_{0.5}Zr_{0.5}O_2$ being highly sensitive to stress variations in mechanical boundary condition, it is reasonable to conclude that stress relaxation over the release process results in a lower total percentage of polar orthorhombic phase. This lower percentage of orthorhombic phase in turn decreases k_t^2 as a lower percentage of total transducer volume is polar and therefore capable of electromechanical transduction. Grazing incident x-ray diffraction (GIXRD) can be used to support this, as polar (111) orthorhombic phase for $Hf_{0.5}Zr_{0.5}O_2$ appears at 30.5º 2θ and is discernible from nonpolar monoclinic $(\bar{1}11)$ at 28.5º 2θ and (111) at 31.9º 2θ when indexed according to existing literature [12][19][20].

Figure 5 (a) shows GIXRD scans taken using a Panalytic X'pert Materials Research Diffractometer (MRD) system with xenon proportional detectors for 2θ varied from 28º to 33º, for released and unreleased ferroelectric $Hf_{0.5}Zr_{0.5}O_2$ samples. Note the clear promotion of nonpolar monoclinic phase upon release of $Hf_{0.5}Zr_{0.5}O_2$. Figure 5 (b-c) depicts unit cells for polar orthorhombic and nonpolar monoclinic phases. The lower percentage of polar phase in released films results in diminished ferroelectricity and is a likely cause for the relatively low exhibited k_t^2, representing a need for further investigation.

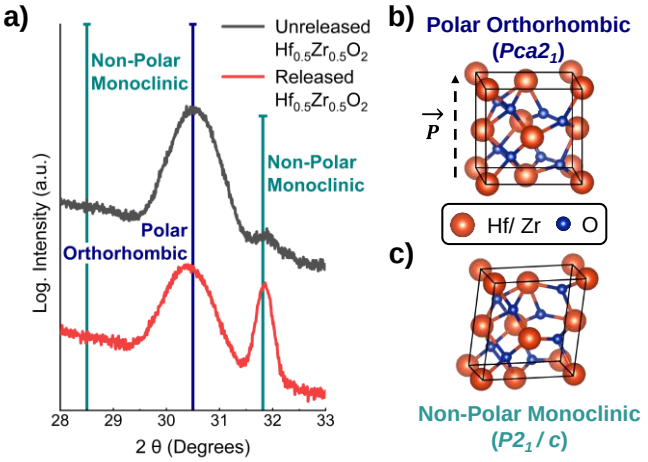

Figure 5. *a) GIXRD scans of released & unreleased, ferroelectric $Hf_{0.5}Zr_{0.5}O_2$ films. Release results in the clear promotion of non-polar, monoclinic phase at 31.8º. b) The polar orthorhombic cell (space group $Pca2_1$) responsible for ferroelectricity in $Hf_{0.5}Zr_{0.5}O_2$. c) The non-polar, monoclinic cell (space group $P2_1/c$).*

CONCLUSION

This work reports the first ever super-high-frequency, ALD hafnia-zirconia resonator, realized via piezoelectric transduction of asymmetric shear-based Lamb-waves at 9.4 GHz. At 0V applied bias, the Lamb-mode resonator achieves a Q of 314.4 and k_t^2 of 0.31%. Additionally, the intrinsic switchability of ferroelectric $Hf_{0.5}Zr_{0.5}O_2$ is demonstrated, with $Hf_{0.5}Zr_{0.5}O_2$ completely depolarizing, and the resonator switching off upon application of 10.5V DC. Comparing on vs off $|Y_{11}|$/ $|Z_{11}|$ yields 7dB of isolation. Further, reasons for lower-than-expected resonator k_t^2 are discussed, with proof found in underlying material morphology.

ACKNOWLEDGEMENTS

This project is supported by DARPA Young Faculty Award program. The authors would like to thank DARPA program manager Dr. Timothy Hancock for his generous support of this work. The authors would also like to thank the University of Florida Nanoscale Research Facility staff for their great help regarding fabrication and material characterization throughout this project.

REFERENCES

[1] H. Bhugra and G. Piazza, *Piezoelectric MEMS resonators*. Springer, 2017.

[2] D. S. Gardner, G. Schrom, F. Paillet, B. Jamieson, T. Karnik, and S. Borkar, "Review of on-chip inductor

structures with magnetic films," *IEEE Trans. Magn.*, vol. 45, no. 10, pp. 4760–4766, 2009, doi: 10.1109/TMAG.2009.2030590.

[3] T. S. Böscke, J. Müller, D. Bräuhaus, U. Schröder, and U. Böttger, "Ferroelectricity in hafnium oxide thin films," *Appl. Phys. Lett.*, vol. 99, no. 10, 2011, doi: 10.1063/1.3634052.

[4] M. Ghatge, G. Walters, T. Nishida, and R. Tabrizian, "An ultrathin integrated nanoelectromechanical transducer based on hafnium zirconium oxide," *Nat. Electron.*, vol. 2, no. 11, pp. 506–512, 2019, doi: 10.1038/s41928-019-0305-3.

[5] M. Ghatge, G. Walters, T. Nishida, and R. Tabrizian, "A Nano-Mechanical Resonator with 10nm Hafnium-Zirconium Oxide Ferroelectric Transducer," *2018 IEEE Int. Electron Devices Meet.*, pp. 4.6.1-4.6.4, 2019, doi: 10.1109/IEDM.2018.8614633.

[6] M. Ghatge, G. Walters, T. Nishida, and R. Tabrizian, "High-Q UHF and SHF Bulk Acoustic Wave Resonators with Ten-Nanometer Hf0.5Zr0.5O2 Ferroelectric Transducer," *2019 20th Int. Conf. Solid-State Sensors, Actuators Microsystems Eurosensors XXXIII (TRANSDUCERS EUROSENSORS XXXIII)*, pp. 446–449, 2019, doi: 10.1109/TRANSDUCERS.2019.8808308.

[7] J. Lyu, T. Song, I. Fina, and F. Sánchez, "High polarization, endurance and retention in sub-5 nm Hf0.5Zr0.5O2films," *Nanoscale*, vol. 12, no. 20, pp. 11280–11287, 2020, doi: 10.1039/d0nr02204g.

[8] R. Materlik, C. Künneth, and A. Kersch, "The origin of ferroelectricity in Hf 1−x Zr x O 2 : A computational investigation and a surface energy model," *J. Appl. Phys.*, vol. 117, no. 13, p. 134109, Apr. 2015, doi: 10.1063/1.4916707.

[9] R. Batra, T. D. Huan, J. L. Jones, G. Rossetti, and R. Ramprasad, "Factors Favoring Ferroelectricity in Hafnia: A First-Principles Computational Study," *J. Phys. Chem. C*, vol. 121, no. 8, pp. 4139–4145, 2017, doi: 10.1021/acs.jpcc.6b11972.

[10] M. H. Park *et al.*, "Study on the degradation mechanism of the ferroelectric properties of thin Hf0.5Zr0.5O2 films on TiN and Ir electrodes," *Appl. Phys. Lett.*, vol. 105, no. 7, pp. 0–5, 2014, doi: 10.1063/1.4893376.

[11] T. Shiraishi *et al.*, "Impact of mechanical stress on ferroelectricity in (Hf0.5Zr0.5)O2 thin films," *Appl. Phys. Lett.*, vol. 108, no. 26, pp. 0–5, 2016, doi: 10.1063/1.4954942.

[12] H. J. Kim *et al.*, "Grain size engineering for ferroelectric Hf0.5Zr0.5O2 films by an insertion of Al2O3 interlayer," *Appl. Phys. Lett.*, vol. 105, no. 19, pp. 1–6, 2014, doi: 10.1063/1.4902072.

[13] S. Kirbach, K. Kühnel, and W. Weinreich, "Piezoelectric Hafnium Oxide Thin Films for Energy-Harvesting Applications," *Proc. IEEE Conf. Nanotechnol.*, vol. 2018-July, pp. 2018–2021, 2019, doi: 10.1109/NANO.2018.8626275.

[14] T. Tharpe, F. Hakim, and R. Tabrizian, "In-Plane Bulk Acoustic Resonators Using 50nm-Thick Nano-Laminated Ferroelectric Hf0.5Zr0.5O2," *21st Int. Conf. Solid-State Sensors, Actuators Microsystems, TRANSDUCERS 2021*, pp. 313–316, 2021, doi: 10.1109/Transducers50396.2021.9495745.

[15] G. Walters, A. Shekhawat, S. Moghaddam, J. L. Jones, and T. Nishida, "Effect of in situ hydrogen plasma on the ferroelectricity of hafnium zirconium oxide films," *Appl. Phys. Lett.*, vol. 116, no. 3, 2020, doi: 10.1063/1.5135709.

[16] M. Lederer *et al.*, "On the Origin of Wake-Up and Antiferroelectric-Like Behavior in Ferroelectric Hafnium Oxide," *Phys. status solidi - Rapid Res. Lett.*, vol. 15, no. 5, 2021.

[17] P. D. Lomenzo *et al.*, "Harnessing Phase Transitions in Antiferroelectric ZrO2 Using the Size Effect," *Adv. Electron. Mater.*, vol. 2100556, pp. 1–10, 2021, doi: 10.1002/aelm.202100556.

[18] T. Tharpe, X. Zheng, P. X. Feng, and R. Tabrizian, "Resolving Mechanical Properties and Morphology Evolution of Free-Standing Ferroelectric Hf0.5Zr0.5O2," *Adv. Eng. Mater.*, vol. 2101221, pp. 1–9, 2021, doi: 10.1002/adem.202101221.

[19] A. Phys *et al.*, "Compositional and phase dependence of elastic modulus of crystalline and amorphous Hf 1- x Zr x O 2 thin films Compositional and phase dependence of elastic modulus of crystalline and amorphous Hf 1- x Zr x O 2 thin films," vol. 102901, no. February, 2021, doi: 10.1063/5.0044702.

[20] S. Riedel, P. Polakowski, and J. Müller, "A thermally robust and thickness independent ferroelectric phase in laminated hafnium zirconium oxide," vol. 095123, no. June, 2016, doi: 10.1063/1.4964300.

CONTACT

*Troy Tharpe, tel: +1-321-4329557; ttharpe@ufl.edu.